



Obrabotka metallov -

Metal Working and Material Science

Journal homepage: http://journals.nstu.ru/obrabotka_metallov







Study of abrasive wear resistance of flux-cored wires during surfacing on high-manganese Hadfield steel



Yulia Karlina^{1, a, *}, Vladimir Konyukhov^{2, 3, b}, Tatiana Oparina^{2, c}

¹ National Research Moscow State University of Civil Engineering, 26 Yaroslavskoe Shosse, Moscow, 129337, Russian Federation

² Irkutsk National Research Technical University, 83 Lermontova str., Irkutsk, 664074, Russian Federation

³ Cherepovets State University, 5 Lunacharsky pr., Cherepovets, 162600, Russian Federation

^a  <https://orcid.org/0000-0001-6519-561X>,  jul.karlina@gmail.com; ^b  <https://orcid.org/0000-0001-9137-9404>,  konyukhov_vyu@mail.ru;

^c  <https://orcid.org/0000-0002-9062-6554>,  martusina2@yandex.ru

ARTICLE INFO

Article history:

Received: 14 September 2025

Revised: 03 October 2025

Accepted: 28 October 2025

Available online: 15 December 2025

Keywords:

Plasma boriding

Amorphous boron

Iron borides

Coating

ABSTRACT

Introduction. Austenitic high-manganese steel is commonly used in various railway and mining components, such as crusher plates, where high impact and abrasive resistance and sliding wear resistance are required, as it exhibits a unique combination of high toughness and high work-hardening ability. Therefore, it is important to understand the behavior of wear-resistant materials such as austenitic high-manganese steel under impact and sliding wear. However, this steel has a limitation: it develops its high work-hardening ability only under high impact loads and high-stress conditions. Alternatively, various hardening methods, surfacing, or replacement with low-carbon, high-alloy steels and high-chromium cast irons are used. **The purpose** of this study is to evaluate the abrasive wear resistance of flux-cored wires during surfacing on high-manganese *Hadfield* steel. **Methods and materials.** This study examines surfacing wires whose main alloying elements are chromium, vanadium, and tungsten. The chemical composition of the surfaced samples was determined using a *BRUKER SI TITAN* portable X-ray fluorescence analyzer for metals and alloys. A *Duramin-40 AC3* hardness tester (*STRUERS APS*, Ballerup, Denmark) was used to measure Rockwell hardness. *1.1% C-13% Mn* steel demonstrated an initial bulk hardness of $HRC = 23 \pm 3$. Specimens for microstructural study were selected from cast and surfaced samples. The microstructures were examined by optical microscopy after etching in 2.5% nitric acid solutions, rinsing in methanol, and immersion in 15% *HCl* solution. Impact abrasive wear tests were conducted on a *DUCOM (TR-56-M3)* impact abrasive wear testing machine (made in India). **Results and discussion.** An analysis of a cross-section of a *1.1% C-13% Mn* steel specimen after abrasive wear testing revealed crack propagation beneath the surface of the part, with no visible connection to the surface, indicating that cracks initiated both at and below the surface. The microstructure of the surfaced layers, rich in finely dispersed boron carbides dispersed in the martensitic matrix, combined with a lamellar molybdenum boride phase, suggests that the material surfaced on *Hadfield* steel may possess higher hardness and wear resistance than the base material. Industrial tests of surfaced beaters revealed that the dominant wear mechanisms are micro-cutting, pitting, and micro-fracture (chipping and micro-indentation). Based on the results of the studies of surfacing materials, it can be concluded that wires with chromium content in the range of 3–6% have the characteristics for applications requiring high abrasive wear resistance in the mining industry.

For citation: Karlina Yu.I., Konyukhov V.Yu., Oparina T.A. Study of abrasive wear resistance of flux-cored wires during surfacing on high-manganese Hadfield steel. *Obrabotka metallov (tekhnologiya, oborudovanie, instrumenty) = Metal Working and Material Science*, 2025, vol. 27, no. 4, pp. 287–308. DOI: 10.17212/1994-6309-2025-27.4-287-308. (In Russian).

Introduction

Coal mills are essential components of thermal power plants, used to prepare solid fuels such as peat, lignite, bituminous coal, and anthracite. These mills consist of drills fixed around the perimeter of the disk or mounted on a shaft. The material is ground into dust, which is blown into the combustion chamber of the boiler. Mill shafts are typically manufactured from wear-resistant cast iron or *Hadfield* steel [1–3].

* Corresponding author

Karlina Yulia I., Ph.D. (Engineering), Research Associate
National Research Moscow State Construction University,
26 Yaroslavskoe shosse,
129337, Moscow, Russian Federation
Tel.: +7 914 879-85-05, e-mail: jul.karlina@gmail.com

In the mining industry, components made from *Hadfield* steel are subjected to severe impact and abrasion, creating a significant impetus for a deeper understanding of wear, deformation, and work hardening in various high-manganese steels under high-stress conditions.

The deformation and wear mechanisms in rock crushers and mills can be classified into two primary categories [4–15]: (1) surface deformation under high stress and high strain rates, similar to impact deformation occurring when rock strikes and fragments against the surface, and (2) high-stress abrasive wear caused by the sliding of large and fragmented rock particles across the surface. Materials must endure repeated cycles of these high loads – causing scratching, indentation, impact, and mineral fracture – without premature failure or critically shortened service life. High-strength steels can offer extended service life due to their durability compared to most low-carbon steels or coated structures under such conditions. To this end, various technologies for modification, heat treatment, and surfacing are employed.

Hadfield austenitic high-manganese steel (typically ~1.2% C and ~12% Mn) holds a special place among wear-resistant high-carbon manganese alloys [1–7]. Owing to its high toughness and wear resistance, *Hadfield* steel is widely used in various industrial applications, including components of stone-crushing machinery, railway crossings, excavator bucket teeth, and tracked vehicle components [5–10].

Literature reports indicate that as-cast *Hadfield* austenitic manganese steel contains $(Fe, Mn)_3C$ carbides [1, 2, 7–18]. It is standard industrial practice to dissolve these carbides prior to service through a solution heat treatment, transforming the structure into a fully single-phase austenite. The traditional heat treatment for cast *110G13L* steel blanks, used by most metallurgical companies, involves solution annealing at approximately 1,050 °C for several hours, followed by water quenching.

Analysis of the literature [1, 2, 5–17] reveals a practical challenge in the application of high-manganese steel machine parts: low wear resistance due to insufficient work-hardening capacity under “mild” operating conditions (i.e., low or absent impact loads) [11, 12]. Given this disadvantage, many researchers have explored modifying the manganese content and optimizing heat treatment to improve the in-service hardening properties. Studies on medium-manganese steels (8–12 wt.% Mn) have shown relatively low abrasive wear resistance [13–16]. Mechanical properties and wear resistance can be enhanced by adding alloying elements such as *Ti*, *Cr*, *Mo*, and *V*, which contribute to solid solution and dispersion strengthening [17–22]. The alloying, heat treatment, hardening behavior, and wear resistance of medium-manganese steels have been systematically studied [23–27]. Results indicate that deformation-induced martensitic transformation in medium-manganese steels provides a self-hardening effect under moderate or low applied loads, leading to better wear resistance compared to high-manganese, bainitic, and martensitic steels [23–27].

The effect of aging on the mechanical properties and wear resistance of medium-manganese steel reinforced with $Ti(C, N)$ particles has been investigated [23–25]. These studies analyzed the influence of precipitate morphology, distribution, and volume fraction on microstructure and mechanical properties, described the relationship between mechanical properties and wear mechanisms, and explained the effects of work-hardening mechanisms.

Alloying significantly influences the deformation mechanisms in steel, promoting slip, twinning, or austenite transformation into α' - and/or ε -martensite, depending on the alloy's stacking fault energy (*SFE*) [1, 2]. However, as noted by several authors [6–12], under high strain rate conditions (e.g., strain rates of 10^3 – 10^5 s^{−1}), the mechanical properties and wear resistance of high-manganese steels can change substantially during operation. This must be considered when designing components for applications such as mining machinery. The addition of carbide-forming elements likely increases the abrasion resistance of high-manganese steels but may also reduce their toughness due to grain boundary carbide precipitation. Therefore, many researchers emphasize the need for continued study of the mechanical properties and wear resistance of high-manganese steels to better understand their performance and enable further development [10–24].

In particular, it has been shown that only a surface layer with a depth of 0.2–0.8 mm is exposed to aggressive media in parts operating under wear conditions [10–12]. In such cases, applying an additional wear-resistant coating to the surface of *110G13L* steel parts can be an effective solution.



In recent years, surfacing and additive manufacturing (AM) technologies have been increasingly used to enhance performance by surfacing heterogeneous materials onto the surfaces of metal parts. *Fe-C-Mo-V-B* surfacing compositions are known, developed specifically for rapidly wearing components of various ore-crushing equipment. These are recommended by manufacturers due to their excellent performance compared to *Ni-WC* compositions and lower cost in applications where corrosion resistance is not a primary requirement [15–28].

According to many researchers, the high wear resistance of *Fe-C-Mo-V-B* compositions stems from the high volume fraction of carbides and borides within a martensitic matrix. Strength and crack resistance are attributed to the fine lamellar structure of molybdenum borides and the spherical morphology of vanadium carbides [20–29].

There are known compositions from both domestic and international manufacturers of surfacing wires based on the *Fe-Cr* system, where additional elements such as *W*, *Nb*, *B*, *Si*, etc., are introduced to enhance the abrasive resistance of machine parts in mining equipment [10–20]. However, systematic analyses of the wear resistance of these wires specifically for mining equipment applications are scarcely available in the public domain.

It is known that wear resistance under abrasive and impact-abrasive conditions depends on the microstructure and mass fraction of carbide phases. A coarser microstructure and lower mass fraction of carbides generally lead to greater weight loss [18]. However, controlling the size and distribution of carbides is a significant challenge for *Fe-Cr-C* surfacing alloys due to the brittleness of large primary chromium carbides. In *Fe-Cr-C* system surfacing, primary carbides often form in the surfaced layer, which can impair the interfacial bonding between the carbides and the matrix [19]. Thus, the wear resistance of a surfaced alloy depends on multiple factors, including the type, shape, and distribution of hard phases, as well as the toughness and work-hardening capacity of the matrix [9]. Consequently, it is necessary to investigate the compatibility between carbides and the matrix to establish the relationship between microstructure and wear based on their distribution and morphology.

Borides and carbides are common hard phases in surfaced alloys [20]. It is well-established that borides formed with transition metals have high potential for extreme applications due to their high hardness and excellent resistance to wear, friction, and corrosion [21]. Literature indicates that boron promotes the formation of primary hard phases, such as borides or carbides, and increases their volume fraction [20–27]. Studies have shown that boron directly influences not only carbide formation but also bulk hardness and wear resistance [22]. Surfacing wires with high boride content are widely used for surfacing in various industrial applications via welding or thermal spraying [24].

Currently, a new field known as remanufacturing is developing — the process of restoring end-of-life and used components to a reusable condition [27–35]. Remanufacturing is becoming increasingly important as a key element for achieving resource efficiency in industry and building a circular economy. Additive manufacturing has emerged as a technology enabling the automated repair and restoration of worn, high-value parts to new condition for their next life cycle.

This paper investigates options for surfacing *110G13L* steel with various commercially available surfacing wires recommended by manufacturers to increase abrasive wear resistance. The studied surfaced materials are based on the *Fe-Cr-C* system, with additional elements such as *W*, *Nb*, *B*, *Mo*, *V*, and *Si* introduced to mitigate excessive wear on *Hadfield* steel drill bits used in coal mills. The study analyzes the chemical composition of the surfaced compositions, conducts macro- and microscopic structural examinations, hardness testing, and wear resistance evaluation.

The purpose of this work is to evaluate the abrasive wear resistance of various commercially available surfacing wires when used for surfacing on *Hadfield* high-manganese steel, specifically for real-world operation in coal mills. To achieve this aim, the following **tasks** were addressed:

- Determining the degree of dilution between the surfaced and base metals.
- Conducting metallographic studies of the microstructure of the surfaced samples.
- Assessing the hardness distribution through the depth of the surfaced layer.
- Performing abrasive wear tests on experimental samples surfaced with wires from different manufacturers and conducting industrial trials on surfaced *Hadfield* steel components.



Materials and methods of research

Product information: hammer mill beaters made of 110G13L steel for a tangential hammer mill (Fig. 1). The chemical composition was determined by optical emission spectrometry using an *ARL 3460* spectrometer and is presented in Table 1.



Fig. 1. Original beater component for surfacing

The main alloying elements in the surfaced metal layer of the samples were determined using a *BRUKER S1 TITAN* portable X-ray fluorescence (XRF) analyzer for metals and alloys.

A *Duramin-40 AC3* hardness tester (*STRUERS*, Denmark) was used to measure Rockwell hardness and microhardness at loads ranging from 0.025 to 0.1 kgf. The *110G13L* steel substrate exhibited an initial bulk hardness of $HRC = 23 \pm 2$.

Samples for microstructural examination were extracted from both the cast substrate and the surfaced specimens. The samples were sectioned using a wire electrical discharge machining (EDM) unit to prevent cracking or phase transformations due to heat input during conventional machining. Subsequently, they underwent standard metallographic preparation: mounting, planar grinding, and polishing. The microstructures were examined by optical microscopy using a *Neophot-21* microscope equipped with a digital camera (*Carl Zeiss*, Germany).

Impact-abrasive wear tests were conducted on a *DUCOM TR-56-M3* impact-abrasive wear testing machine (India).

Table 1

Chemical composition of the 1.1% C-13% Mn steel beater according to GOST 977-88

C	Si	Mn	Cr	Ni	Cu	S	P
			no more				
0.90–1.50	0.30–1.00	11.50–15.00	1.00	1.00	0.30	0.05	0.120
1.12 (actual)	0.98	12.34	0.6	0.1	0.2	0.055	0.134

The technical documentation governing the repair of *110G13L* steel plates specifies the following conditions for restoring a worn surface: *T-590* and *T-620* grade electrodes were used, with a maximum of 1-2 layers. *UONI 13/45* electrodes were used for the buffer layer formation.

This study examined several types of surfacing wires (diameter 1.2–1.6 mm) available on the Russian market:

1. *ASM 57-OA*, Russian Federation.
2. *TD-600*, Italy, manufacturer *Italfil*.
3. *TD-RC3*, Italy, manufacturer *Italfil*.
4. *CARBO AF D600*, Germany, manufacturer *CarboWeld*.
5. *K-600NT*, *Kiswel*, South Korea.
6. *K-700NT*, *Kiswel*, South Korea.
7. *OK Tubrodur 58 O/GM*, *ESAB*, manufactured in Poland.

SV-08Kh18Ni10T (0.08% C-18% Cr-10% Ni-1% Ti) welding wire (Russian Federation) was used as a buffer layer, which was pre-surfaced onto the *110G13L* steel surface prior to surfacing.

The chemical compositions of the aforementioned surfacing wires are presented in Table 2. The surfacing parameters for the samples are detailed in Fig. 2 and Table 3.

Sample No. 1 was surfaced using *ASM 57-OA* wire (\varnothing 1.6 mm). According to Table 2, this wire contains 0.80% C, up to 18% Cr, and up to 2% B, which increases the susceptibility of the surfaced metal to cracking. To minimize cracking, preheating to 180 °C was applied, and the interpass temperature was maintained

Table 2

Chemical composition of the investigated surfacing wire grades

Chemical element	Wire grade						
	ACM 57-OA	TD-600	TD-RC3	CARBO AF D600	K-700HT	K-600HT	OK Tubrodur 58 O/GM ESAB
C	0.8	0.15	0.37	0.5	0.3	0.25	0.42
Si	1	3	0.4	2.7	2.4	2.18	0.31
Mn	2	0.1	1.1	0.5	0.5	0.36	1.22
Cr	18	9.3	7	9.5	7	6.5	4.89
B	2.6						
P		<0.025	<0.03				
S		<0.020	<0.020				
Cu		<0.25	<0.25				
Ni		<0.15	<0.20				
V		<0.030					
Al		<0.030					0.6
Mo			2.2			0.5	1.14
Ti			0.3				
W					0.7		



Fig. 2. Wire surfaced samples

Table 3

Surfacing parameters

Surfacing material	Current, A	Voltage, V	Wire feed speed mm/sec
ACM 57-OA	258	29.5	9.1
TD-RC3	258	23.2	9.6
TD-600	258	27.0	5.5
CARBO AF D600	260	28.5	5.6
K-700HT	260	28.0	5.6
K-600HT	260	28.0	5.6

in the range of 250–270 °C. Temperature was monitored with an ADA TemPro 900 A00225 non-contact thermometer with a measurement error of ± 15 °C.

Sample No. 2 was surfaced using TD-RC3 wire (\varnothing 1.6 mm).

Sample No. 3 was surfaced using TD-600 wire (\varnothing 1.6 mm).

Sample No. 4 was surfaced using T-590 electrodes (\varnothing 4.0 mm).

Sample No. 5 was surfaced using *CARBO AF D600* wire (\varnothing 1.6 mm). To minimize cracking, preheating to 180 °C was applied, and the interpass temperature was maintained at 250–270 °C. Temperature was monitored with the same ADA thermometer.

Sample No. 6 was surfaced using *K-600NT* wire (\varnothing 1.6 mm).

Sample No. 7 was surfaced using *K-700NT* wire (\varnothing 1.6 mm).

Surfacing was performed using *LORCH P5500 MIG/MAG* welding equipment: an industrial semi-automatic welding system *P 5500 Speed XT*, a compact power source with water cooling, integrated wire feeder and control panel, an *SB 550W* liquid-cooled welding torch (550A for CO_2 / 500A for Ar/CO_2 , 100% duty cycle, for 1.2–1.6 mm wire), equipped with an ergonomic handle and Euro connector.

Research results

Prior to surfacing on the experimental batch of hammers (beat), incoming inspection of the cast products was performed:

- Items were numbered and documented with photographs (Figs. 3–5);
- Surfaces were cleaned using mechanical tools on three sides;
- Weighing was conducted.

Visual and penetrant testing of the seven received products revealed the defects listed in Table 4.

A milling operation of the working surface was performed to a depth of 10 mm. Extensive through-hole defects were identified on two hammers (No. 1 and 3). Subsequently, new hammer samples were selected for surfacing, which successfully passed visual and capillary control.

Preliminary studies were conducted on witness (test) samples to determine the microstructure in the surfaced layer, measure hardness, and evaluate wear resistance.



Fig. 3. Visual inspection of the beater surface after removal of metallurgical slag



Fig. 4. Penetrant testing



Fig. 5. Extended through-thickness defects on the beater, numbered 1, 3 (see Fig. 3)

Table 4

Defects identified by visual and liquid penetrant testing

Product number	Identified defects
1	Pores and a shrinkage cavity in the working section of the component
2	Pores and micro-cracks on the surface
3	Pores and cracks extending to the surface. After sectioning 7 mm deep, a shrinkage void was observed in the functional area of the part
4	Pores and cracks extending to the surface
5	Pores extending to the surface
6	Pores extending to the surface
7	Pores extending to the surface

Metallographic Studies

Fig. 6 shows the microstructure of cast *110G13L* steel, where non-metallic inclusions and carbides along grain boundaries are clearly visible. Examination of the heat-affected zone (*HAZ*) revealed a fully austenitic microstructure with a high density of deformation slip bands and twinning within the grains, indicating

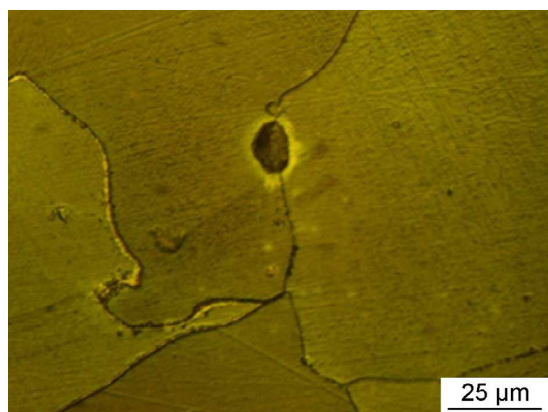
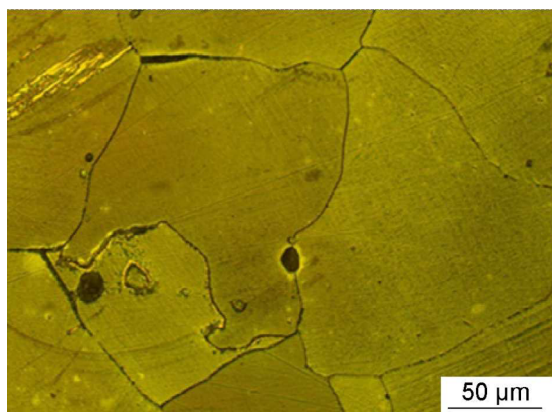


Fig. 6. Carbides at austenite grain boundaries and non-metallic inclusions

significant work hardening. Additionally, cracks propagating along some austenitic grain boundaries were observed in several sections, while other grain boundaries remained intact.

The microstructure of the surfaced layers is shown in Figs. 7–8. The structure of the surfaced metal contains boron carbides (Figs. 8, *a, b*) and chromium carbides (Figs. 8, *c, d*).

The chemical composition of the surfaced layers, determined using the *Bruker SI TITAN* fluorescence spectrometer, is presented in Tables 5–10. The main alloying elements are chromium, molybdenum, manganese, and vanadium. Titanium (declared by the manufacturer for *CARBO AF D600* wire) and tungsten (declared for *K-700NT*) were not detected in the surfaced metal.

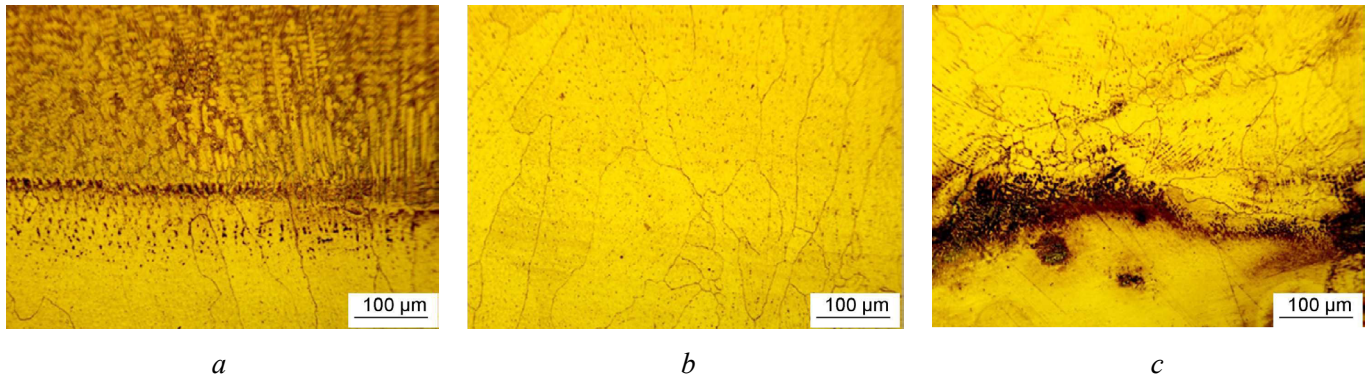


Fig. 7. Microstructure of the surfaced layer with a buffer layer:

a – surfaced layer at the boundary with the buffer layer; *b* – buffer layer; *c* – transition layer between the buffer layer and 1.1% C-13% Mn steel

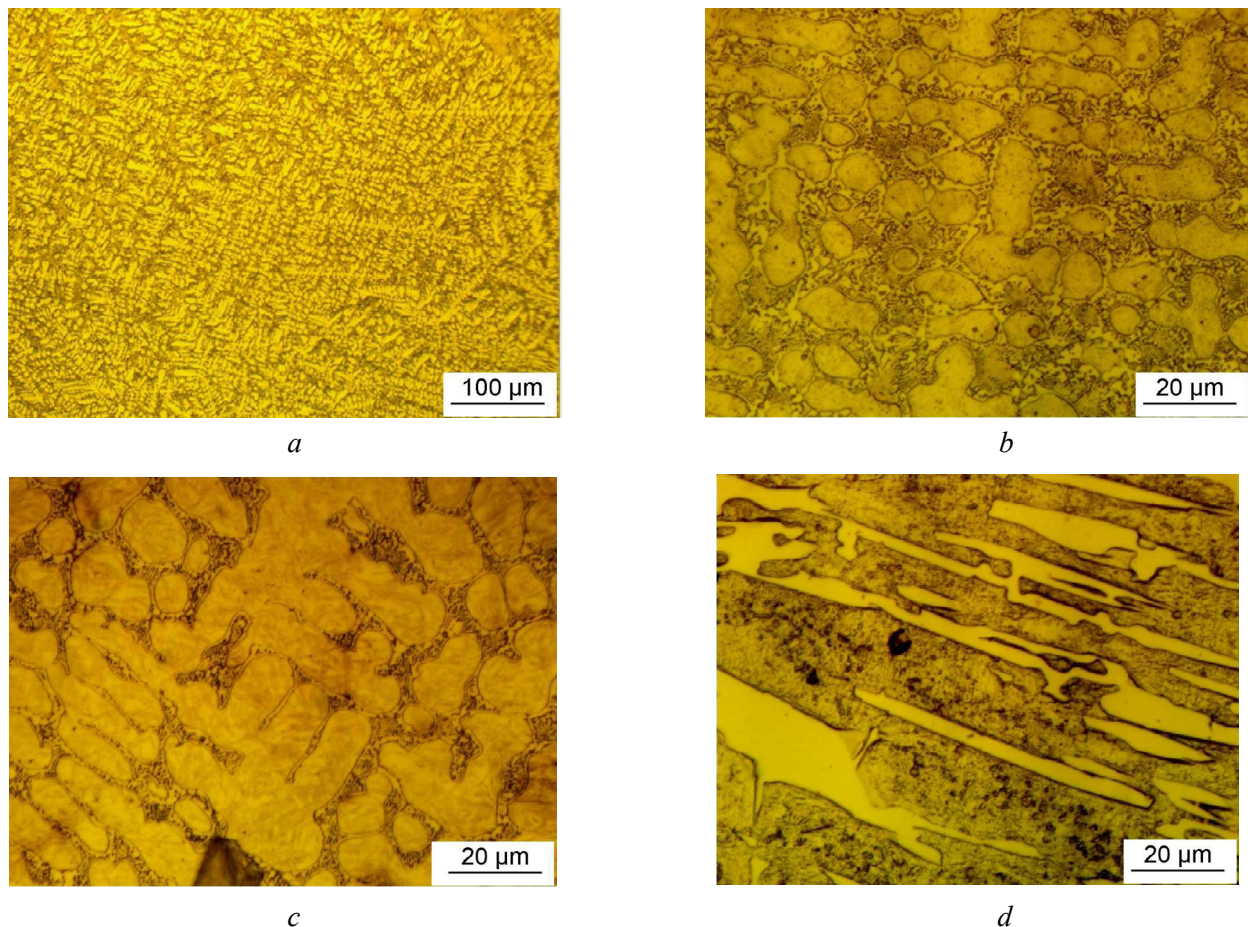


Fig. 8. Microstructure of surfaced layers:

a – surfaced layer with ASM 57 – OA wire; *b* – surfaced layer with CARBO AF D600 wire; *c* – surfaced layer with TD-RC3 wire; *d* – surfaced layer with TD-600 wire

Table 5

Chemical composition of the layer surfaced with T-590 wire. %

<i>Mn</i>	<i>Cr</i>	<i>Si</i>	<i>Cu</i>	<i>Ni</i>	<i>Mo</i>
6.23	4.29	2.0	0.07	0.06	0.02

Table 6

Chemical composition of the layer surfaced with ASM 57 – OA wire

<i>Mn</i>	<i>Cr</i>	<i>Si</i>	<i>Ni</i>	<i>B</i>	<i>Cu</i>
6.00	8.32	0.43	0.07	0.16	0.05

Table 7

Chemical composition of the layer surfaced with TD-RC3 wire

<i>Cr</i>	<i>Mn</i>	<i>Mo</i>	<i>Si</i>	<i>Cu</i>	<i>S</i>	<i>Ni</i>
5.32	2.94	1.61	0.51	0.36	0.24	0.22

Table 8

Chemical composition of the layer surfaced with TD-600 wire

<i>Cr</i>	<i>Mn</i>	<i>Si</i>	<i>Cu</i>	<i>Ni</i>	<i>Mo</i>
7.18	2.93	2.36	0.29	0.12	0.02

Table 9

Chemical composition of the layer surfaced with CARBO AF D600 wire

<i>Cr</i>	<i>Mn</i>	<i>Si</i>	<i>Cu</i>	<i>Ni</i>
8.18	0.53	0.36	0.29	0.12

Table 10

Chemical composition of the layer surfaced with K-700NT wire

<i>Mn</i>	<i>Cr</i>	<i>Si</i>	<i>Cu</i>	<i>Ni</i>
4.23	6.29	2.0	0.07	0.06

All wires demonstrate chromium as the primary alloying element, differing only in its concentration in the surfaced metal (see Tables 5–10). Notably, the manufacturer's certificate for *ASM 57-OA* wire stated a chromium content of 18%, whereas the actual chromium content in the surfaced metal was 2.2 times lower (Table 6).

The results of macrohardness measurements on the surface of the surfaced samples are shown in Table 11. Three measurements were taken at different points on the surfaced surface, showing that hardness is uniformly distributed across the surfaced metal.

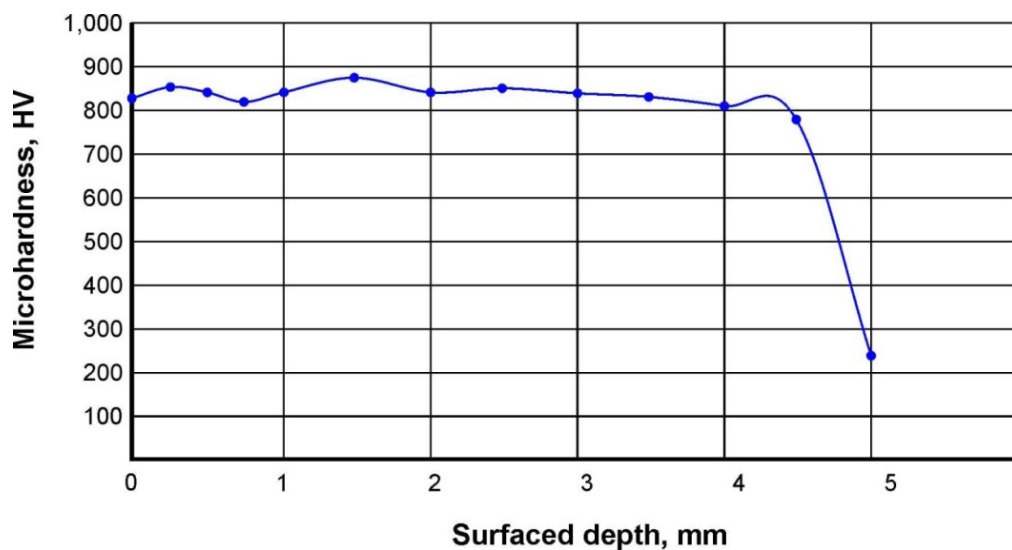
Fig. 9 graphically presents the results of microhardness distribution measurements across the depth of the surfaced layer.

The results of the abrasion resistance test are shown in Fig. 10. Initially, it can be confirmed that all surfacing materials used for surfacing exhibited lower mass loss during testing compared to samples of the base *Hadfield* steel. In terms of mass loss, wires designated in Fig. 10 as **No. 7 – K-600NT** and **No. 8 – K-700NT** demonstrated the lowest values.

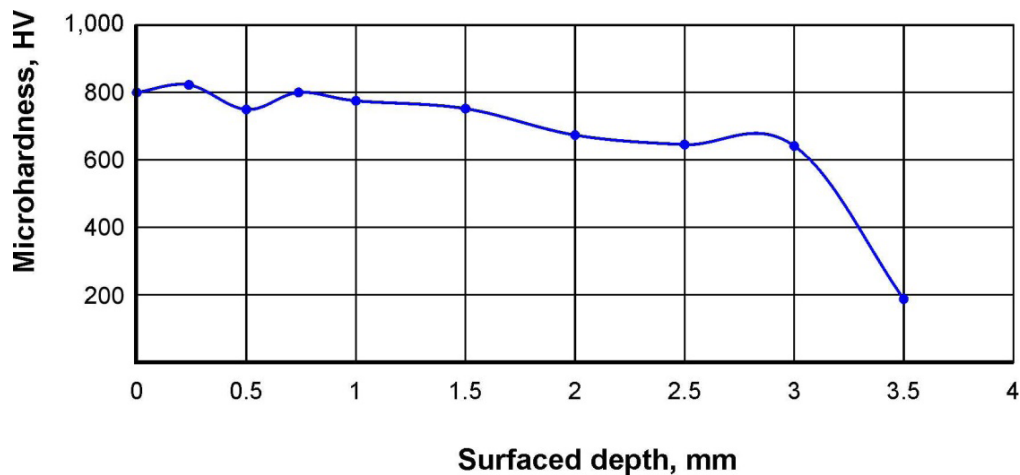
Table 11

Rockwell hardness of the surfaced layer of samples, HRC

Sample name	Hardness 1	Hardness 2	Hardness 3	Average value
<i>ACM 57 – OA</i>	48.5	50	51	49.83
<i>TD-RC3</i>	45.5	46.0	48	46.5
<i>TD-600</i>	50	51	51	50.66
<i>CARBO AF D600</i>	55	54	58	56.5
<i>K-600HT</i>	58	55	59	57.5
<i>K-700HT</i>	61	61.5	61	61
<i>T-590</i>	40	42	44	42



a



b

Fig. 9. Microhardness profiles across the surfaced depth:

a – K-700NT wire; b – TD-600 wire

Subsequently, a batch of 12 hammers (Fig. 11), surfaced with K-700NT wire, was installed on the *MMT-1A* mill. The remaining rows were fitted with standard, non-surfaced *110G13L* steel hammers in the quantity of 114 pieces (Fig. 12). After 466 hours of testing, an inspection was conducted (Fig. 13). Following this inspection, testing was continued until the hammers were completely worn out.

Fig. 10. Abrasive wear test results (mass loss of surfacing wires):

1 – Hadfield steel; 2 – ASM 57 – OA; 3 – T590; 4 – TD-RC3; 5 – CARBO AF D600; 6 – TD-600; 7 – K-600NT; 8 – K-700NT

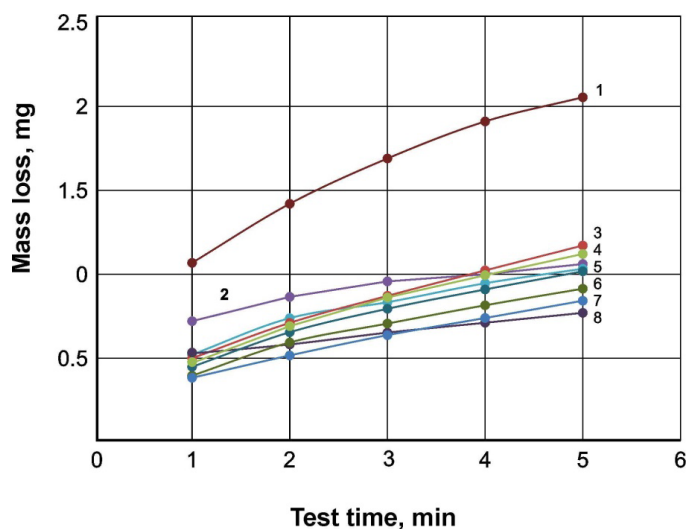


Fig. 11. Surfaced beaters for mill mounting



Fig. 12. Placement of beaters in the mill

Discussion of the results

Studies have shown that the microstructure of the surfaced metal is based on martensite and carbides of the M_3C , M_7C_3 , and $M_{23}C_6$ types. Borides are observed in the microstructure of the deposit from ASM 57-OA wire (Fig. 8, a). The high carbon content in the wires ASM 57-OA, TD-RC3, CARBO AF D600, and K-600NT promotes the formation of a martensitic matrix with inclusions of γ (Fig. 8, d). The martensitic microstructure is often chosen for its excellent abrasion resistance and satisfactory impact toughness.

Analyzing the average hardness and microhardness values measured along the cross-section of the surfaced beads, it can be noted that hardness values were in the range of 720–900 HV, except for the sample surfaced with TD-RC3 wire, which had a hardness of approximately 46.5 HRC (equivalent to ~460 HV).

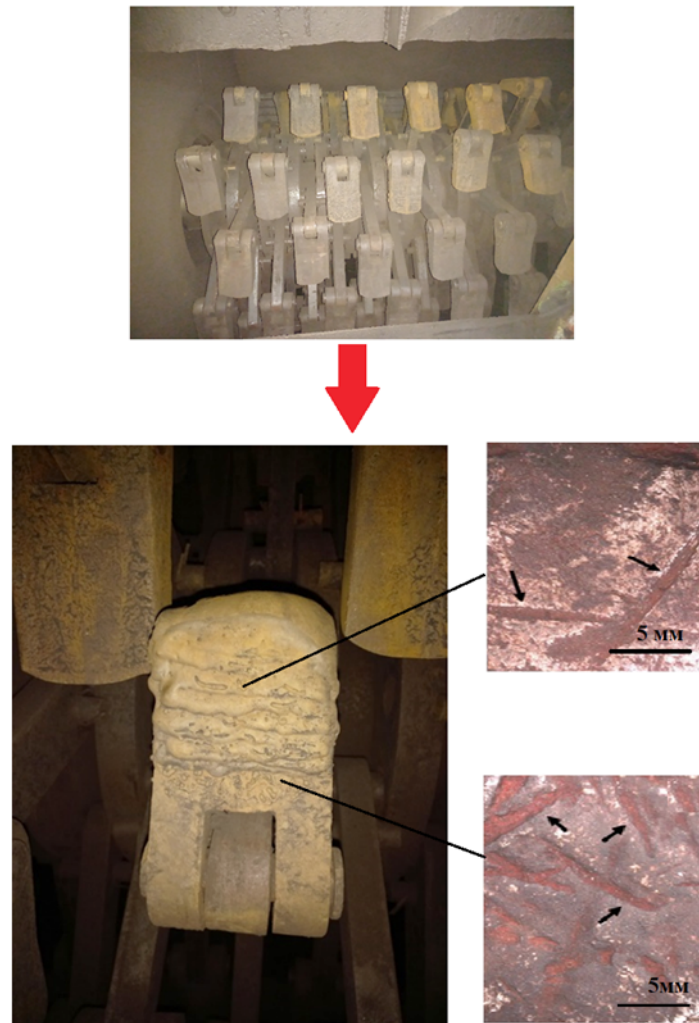


Fig. 13. Inspection of welded beaters after 466 hours of testing

These values are significantly higher than those of the Hadfield steel substrate, which measured 258 HV. The microhardness profile measured through the depth of the coating is shown in Fig. 9. The depth of the surfaced layers is 3–4 mm. The hardness in the middle of the coating averaged 750 HV, while the highest hardness values were recorded in the top layer of the coating. Figure 9 shows a peak microhardness of 900 HV for two samples. The higher hardness of the coating is attributed to the formation of a large number of primary M_7C_3 carbides and may also be associated with the martensitic phase. In the case of the *TD-RC3* wire (Fig. 10, *b*), the hardness is lower, which correlates with a relatively lower concentration of elements such as Cr and C in the surfaced metal. Thus, it can be inferred that the type, size, shape, and distribution of carbides, as well as the matrix structure, strongly influence the hardness of the surfaced layer.

It should be noted that, regardless of the surfacing material used, the thermal conditions during deposition did not alter the microstructure to an extent that would significantly change the hardness of the surfaced beads. Furthermore, the hardness of the surfaced beads is approximately twice as high as that of the *110G13L* steel substrate, suggesting greater wear resistance compared to the substrate. The increase in hardness relative to the substrate can be explained by the volume fraction of carbides distributed in the matrix phase [12, 36–37]. The ratio of carbide to matrix volume plays an important role in wear resistance. A coating with a higher volume fraction of carbides exhibits greater wear resistance, which also correlates with higher hardness [20–24, 38–40].

In our studies of standard *110G13L* steel plates surfaced with various wires exhibiting different chemical compositions and high hardness, some explanation of the obtained results is required. It is known that the hardness of both the matrix and the carbide phase determines the overall hardness of the surfaced layer. The

hardness of alloy steels can generally serve as an indicator of abrasive wear resistance [24, 41–42]. Wear resistance typically increases with hardness [25]. The authors of [26] reported that the wear resistance of $Ni_3Al-M_7C_3$ carbide coatings improved significantly due to the presence of hard phases in a ductile matrix.

In our case, carbides are embedded in a hard (martensitic) matrix. According to the results of our hardness measurements and abrasive wear tests, a correlation exists between hardness and wear resistance, as surfaced samples with hardness ranging from 500 to 1,000 HV showed 30–50% higher resistance to abrasion compared to 110G13L steel samples (Fig. 10). Since mass loss was low for all surfaced samples, the sensitivity of the test must also be considered; thus, it can be stated that all samples performed similarly, as observed in other studies [19–24, 43–45]. Carbides protruding above the surface can temporarily protect it from further wear by preventing direct contact between the sample surface and the abrasive. Protruding carbides can also serve as sites for the accumulation and compaction of wear debris, contributing to the formation of a stable protective tribolayer [19–20].

Analysis of the cross-section of a 110G13L steel sample after industrial abrasive wear testing by coal particles revealed subsurface cracks with no visible connection to the surface. The authors of [20] conducted a systematic analysis of the significance of carbide inclusions for assessing the impact toughness of three steel types: manganese steel (Grade B3), high-carbon steel (Grade B4), and chromium steel (Grade C). They reported that the degree of embrittlement in austenitic manganese steels depends on the extent of grain boundary coverage by brittle phases. Thin carbides (thickness $< 0.2 \mu\text{m}$) and thick carbides (thickness $\sim 0.5\text{--}1.5 \mu\text{m}$) were classified, with the latter being more detrimental, especially in large weld deposits [20].

In the present study, many cracks were found in areas with carbides larger than $0.2 \mu\text{m}$, and others propagated where carbide inclusions were smaller than $0.2 \mu\text{m}$. This suggests that under the combined impact and abrasion conditions in which the 110G13L steel component operates, merely having carbide inclusions smaller than $0.2 \mu\text{m}$ is insufficient; it is necessary to prevent or eliminate carbide precipitation at grain boundaries. This finding motivates our further research into heat treatment to meet the impact and abrasion resistance requirements for coal mill hammer components.

Fig. 13 shows the worn surface of a crusher segment (upper part) examined using a stereo microscope. Deformation marks are clearly visible during macroscopic examination. These marks resemble wear patterns resulting from significant particle impacts on the surface. The authors of [22] classified wear caused by repeated solid particle impact as impact wear. However, the synergistic effect between impact and abrasion, referred to in the literature as impact-abrasion, has been described by several authors [12–20]. The observed damage mechanisms on worn hammers operating on coal ash led us to conclude that impact damage mechanisms, synergistically interacting with abrasion mechanisms, create resultant wear rates exceeding the sum of individual components, consistent with the results of other work [16–23]. It is important to emphasize that the observed wear features (see Fig. 12) exceed the material's grain size, suggesting that the material removal process occurs on a millimeter scale. Therefore, given the nature of this phenomenon involving the grinding of abrasive coal fragments and impact between metal bodies, the term “impact-abrasive wear” better describes the mechanism considered in this study.

To compare the wear resistance of surfacing materials with various microstructures, including some in different deformed states, the wear rate can be expressed as wear per unit of impact energy [23]. It should be noted that during impact, energy is also dissipated in other processes (e.g., friction). In [23], energies dissipated during impact were calculated individually from high-speed images of each test. According to the authors, representing wear rates based on dissipated energy and the mass of erosive particles can provide a more accurate assessment of wear test results.

In conclusion, industrial tests of surfaced hammers have demonstrated a significant increase in service life compared to non-surfaced hammers. Evaluation of the abrasive wear resistance of the investigated welding wires from various manufacturers shows similar results. All investigated wires possess characteristics that allow their use for surfacing coatings on components made of 110G13L steel in mining equipment or other applications requiring high wear resistance.

Conclusions

1. Analysis of the cross-sections for all investigated welding wires revealed that dilution between the surfaced layer and the substrate is minimal. Higher heat input from the welding arc typically results in the formation of higher and wider weld beads, whereas lower heat input values can lead to incomplete fusion or bead detachment. The presence of cracks was noted in some samples, with their propagation arrested within the buffer (buttering) layer.

2. Microstructural analysis demonstrated that the surfaced layer consists of carbide inclusions (chromium, iron, and boron-based) embedded within a martensitic matrix. During the surfacing process, grains in regions closer to the substrate interface were finer than those on the surface. This is attributed to a higher cooling rate near the interface, which suppresses grain growth.

3. The microhardness of all studied surfacing wires ranged from 550 to 900 HV, which is 2–3 times higher than the microhardness of the base *110G13L* steel (approximately 250 HV). This high hardness is attributed to the significant volume fraction of chromium carbides within the surfaced metal.

4. Abrasive wear resistance tests indicated that all samples, with chromium content in the surfaced metal ranging from 4.3 to 8.4 wt.%, exhibited comparable wear resistance. Industrial field trials of surfaced hammers (beaters) under actual coal grinding conditions at a thermal power plant demonstrated a 40–50% increase in service life compared to standard, non-surfaced *110G13L* steel beaters.

References

1. Tweedale G., Paton W.D.M. Sir Robert Abbott Hadfield F.R.S (1858–1940) and the discovery of manganese steel. *Notes and Records of the Royal Society of London*, 1985, vol. 40 (1), pp. 63–74.
2. Gauzzi F., Rossi M., Verdini B. Cold-working induced martensitic transformation in 12 percent Mn austenitic steel (Hadfield steel). *Metallurgia Italiana*, 1971, vol. 63 (11), p. 555.
3. Dastur Y.N., Leslie W.C. Mechanism of work hardening in Hadfield manganese steel. *Metallurgical Transactions A*, 1981, vol. 12 (5), pp. 749–759. DOI: 10.1007/BF02648339.
4. Bhattacharyya S. A friction and wear study of Hadfield manganese steel. *Wear*, 1966, vol. 9 (6), pp. 451–461. DOI: 10.1016/0043-1648(66)90136-0.
5. Lindroos M., Apostol M., Heino V., Valtonen K., Laukkanen A., Holmberg K., Kuokkala V.T. The deformation, strain hardening, and wear behavior of chromium-alloyed Hadfield steel in abrasive and impact conditions. *Tribology Letters*, 2015, vol. 57 (3), p. 24. DOI: 10.1007/s11249-015-0477-6.
6. Ten E.B., Bazlova T.A., Likhobov E.Yu. Vliyanie vnepechnoi obrabotki na strukturu i mekhanicheskie svoystva stali 110G13L [Effect of out-of-furnace treatment on the structure and mechanical properties of steel 110G13L]. *Metallovedenie i termicheskaya obrabotka metallov = Metal Science and Heat Treatment*, 2015, no. 3, pp. 26–28. (In Russian).
7. Bolobov V.I., Bochkov V.S., Qinyan X. Iznosostoykost' stali Gadfil'da pri bol'shikh udel'nykh nagruzkakh [The influence of high specific loads to wear resistance of Hadfield steel]. *Gornoe oborudovanie i elektromekhanika = Mining Equipment and Electromechanics*, 2012, no. 10, pp. 12–14.
8. Kolokoltsev V.M., Vdovin K.N., Chernov V.P., Feoktistov N.A., Gorlenko D.A., Dubrovin V.K. Issledovanie mekhanizmov abrazivnogo i udarno-abrazivnogo iznashivaniya vysokomargantsevoi stali [Study of abrasive and impact and abrasive wear mechanisms of high manganese steel]. *Vestnik Magnitogorskogo gosudarstvennogo tekhnicheskogo universiteta im. G.I. Nosova = Vestnik of Nosov Magnitogorsk State Technical University*, 2017, no. 2, pp. 54–62. DOI: 10.18503/1995-2732-2017-15-2-54-62.
9. Chorshanbiev Sh.M., Karimov K.A., Adilova Sh.R., Turakhodjaev N.J., Erkinjonov A., Mirmuhamedov M.M., Sharipov J.H., Obidov Z.R., Komolov Kh. Development of wear-resistant parts of high-manganese modified 110G13L brand steel. *Zhurnal Sibirskogo federal'nogo universiteta. Tekhnika i tekhnologii = Journal of Siberian Federal University. Engineering & Technologies*, 2024, vol. 17 (2), pp. 175–185.
10. Bolobov V.I., Chupin S.A. Vliyanie vida uprochnyayushchei obrabotki na iznosostoykost' materialov gornogo oborudovaniya [Influence of the type of hardening treatment on the wear resistance of mining equipment materials]. *Zapiski Gornogo instituta = Journal of the Mining institute*, 2015, vol. 216, pp. 44–48.
11. Bolobov V.I., Batalov A.P., Bochkov V.S., Chupin S.A. Iznosostoykost' stali 110G13L v razlichnykh abrazivnykh sredakh [Wear resistance of 110G13L steel in various abrasive environments]. *Zapiski Gornogo instituta = Journal of the Mining institute*, 2014, vol. 209, pp. 17–22.



12. Balanovsky A.E., Shtayger M.G., Grechneva M.V., Kondrat'ev V.V., Karlina A.I. Comparative metallographic analysis of the structure of St3 steel after being exposed to different ways of work-hardening. *IOP Conference Series: Materials Science and Engineering*, 2018, vol. 411 (1), p. 012012. DOI: 10.1088/1757-899X/411/1/012012.
13. Teplukhin V.G., Popov A.I., Kudryavtsev V.N., Fomin D.S., Radkevich M.M. Features of investigation of steels with a metastable austenitic structure. *Advances in Mechanical Engineering: Selected contributions from the conference "Modern engineering: Science and education"*, Saint Petersburg, Russia, June 2022. Cham, Springer Nature Switzerland, 2023, pp. 164–171. DOI: 10.1007/978-3-031-30027-1_18.
14. Filippov M.A., Shveikin V.P., Sharapova V.A., Nikiforova S.M., Khadyev M.S. Formation of a dissipative structure of metastable austenite for raising the wear resistance of carbon steels. *Metal Science and Heat Treatment*, 2023, vol. 64 (9), pp. 509–515. DOI: 10.1007/s11041-023-00854-w.
15. Vdovin K., Pesin A., Feoktistov N., Gorlenko D. Surface wear in Hadfield steel castings DOPED with ni-trided vanadium. *Metals*, 2018, vol. 8 (10), p. 845. DOI: 10.3390/met8100845.
16. Kondrat'ev V.V., Gorovoy V.O., Kolosov A.D., Kononenko R.V., Konyukhov V.Y. Description of the complex of technical means of an automated control system for the technological process of thermal vortex enrichment. *Journal of Physics Conference Series*, 2020, vol. 1661 (1), p. 012101. DOI: 10.1088/1742-6596/1661/1/012101.
17. Kozyrev N., Usoltsev A., Kryukov R., Gusev A., Osetkovskiy I. Operational factors of new flux cored wires of the Fe–C–Si–Mn–Cr–Ni–Mo system for surfacing of protective plates of shearer cutting drums. *IOP Conference Series: Earth and Environmental Science*, 2019, vol. 377, p. 012022. DOI: 10.1088/1755-1315/377/1/012022.
18. Kozyrev N., Usol'tsev A., Kryukov R., Gusev A., Osetkovskii I. Ekspluatatsionnye pokazateli novykh poroshkovykh provolok sistemy Fe–C–Si–Mn–Cr–Ni–Mo [Operation indices of the new cored wire of Fe–C–Si–Mn–Cr–Ni–Mo system]. *Chernaya metallurgiya. Byulleten' nauchno-tekhnicheskoi i ekonomicheskoi informatsii = Ferrous Metallurgy. Bulletin of Scientific, Technical and Economic Information*, 2019, vol. 75, no. 7, pp. 860–869.
19. Gusev A.I., Kibko N.V., Popova M.V., Kozyrev N.A., Osetkovskii I.V. Naplavka poroshkovymi provolokami sistem C–Si–Mn–Mo–V–V i C–Si–Mn–Cr–Mo–V detalei gornorudnogo oborudovaniya [Surfacing of details of mining equipment by powder wires of C–Si–Mn–Mo–V–B and C–Si–Mn–Cr–Mo–V systems]. *Izvestiya vysshikh uchebnykh zavedenii. Chernaya Metallurgiya = Izvestiya. Ferrous Metallurgy*, 2017, vol. 60, no. 4, pp. 318–323. DOI: 10.17073/0368-0797-2017-4-318-323.
20. Shlyakhova G.V., Danilov V.I. Issledovanie vliyaniya elektrodugovoi naplavki na strukturu i svoistva pokrytii [Effect of electric arc surfacing on the structure and properties of coatings]. *Izvestiya vysshikh uchebnykh zavedenii. Chernaya Metallurgiya = Izvestiya. Ferrous Metallurgy*, 2024, vol. 67, no. 4, pp. 433–439. DOI: 10.17073/0368-0797-2024-4-433-439.
21. Metlitskii V.A. Flux-cored wires for arc welding and surfacing of cast iron. *Welding International*, 2008, vol. 22 (11), pp. 796–800. DOI: 10.1080/09507110802593646.
22. Mutaşcu D., Karancı O., Mitelea I., Crăciunescu C.M., Buzdugan D., Uțu I.D. Pulsed TIG cladding of a highly carbon-, chromium-, molybdenum-, niobium-, tungsten- and vanadium-alloyed flux-cored wire electrode on duplex stainless steel X2CrNiMoN 22-5-3. *Materials*, 2023, vol. 16 (13), p. 4557. DOI: 10.3390/ma16134557.
23. Świerczyńska A., Varbai V., Pandey Ch., Fydrych D. Exploring the trends in flux-cored arc welding: scientometric analysis approach. *The International Journal of Advanced Manufacturing Technology*, 2024, vol. 130 (1), pp. 87–110. DOI: 10.1007/s00170-023-12682-6.
24. Golyakevich A.A., Orlov L.N., Maksimov S.Yu. Peculiarities of welding process using metal cored wire of TMV5-MK grade. *The Paton Welding Journal*, 2019, vol. 6, pp. 50–53. DOI: 10.15407/tpwj2019.06.10.
25. Sabzi M., Obeydavi A., Mousavi Anijdan S.H. The effect of joint shape geometry on the microstructural evolution, fracture toughness, and corrosion behavior of the welded joints of a Hadfield steel. *Mechanics of Advanced Materials and Structures*, 2018, vol. 26 (12), pp. 1053–1063. DOI: 10.1080/15376494.2018.1430268.
26. Eremin E.N., Losev A.S. A flux-core wire for hardfacing sealing surfaces of stop valves. *Welding International*, 2016, vol. 30 (3), pp. 216–219. DOI: 10.1080/09507116.2015.1044268.
27. Kanishka K., Acherjee B. A systematic review of additive manufacturing-based remanufacturing techniques for component repair and restoration. *Journal of Manufacturing Processes*, 2023, vol. 89, pp. 220–283. DOI: 10.1016/j.jmapro.2023.01.034.
28. Lee C.M., Woo W.S., Roh Y.H. Remanufacturing: Trends and issues. *International Journal of Precision Engineering and Manufacturing-Green Technology*, 2017, vol. 4 (1), pp. 113–125. DOI: 10.1007/s40684-017-0015-0.
29. Konstantinova M.V., Balanovskiy A.E., Gozbenko V.E., Kargapol'tsev S.K., Karlina A.I., Shtayger M.G., Guseva E.A., Kuznetsov B.O. Application of plasma surface quenching to reduce rail side wear. *IOP Conference Series: Materials Science and Engineering*, 2019, vol. 560 (1), p. 012146. DOI: 10.1088/1757-899X/560/1/012146.



30. Yelemessov K., Baskanbayeva D., Martyushev N.V., Skeebe V.Y., Gozbenko V.E., Karlina A.I. Change in the properties of rail steels during operation and reutilization of rails. *Metals*, 2023, vol. 13 (6), p. 1043. DOI: 10.3390/met13061043.
31. Shtayger M.G., Balanovskiy A.E., Kargapoltsev S.K., Gozbenko V.E., Karlina A.I., Karlina Yu.I., Govorkov A.S., Kuznetsov B.O. Investigation of macro and micro structures of compounds of high-strength rails implemented by contact butt welding using burning-off. *IOP Conference Series: Materials Science and Engineering*, 2019, vol. 560 (1), p. 012190. DOI: 10.1088/1757-899X/560/1/012190.
32. Balanovskiy A.E., Shtayger M.G., Karlina A.I., Kargapoltsev S.K., Gozbenko V.E., Karlina Yu.I., Govorkov A.S., Kuznetsov B.O. Surface hardening of structural steel by cathode spot of welding arc. *IOP Conference Series: Materials Science and Engineering*, 2019, vol. 560 (1), p. 012138. DOI: 10.1088/1757-899X/560/1/012138.
33. Skeebe V.Yu., Ivancivsky V.V., Kutyskhin A.V., Parts K.A. Hybrid processing: the impact of mechanical and surface thermal treatment integration onto the machine parts quality. *IOP Conference Series: Materials Science and Engineering*, 2016, vol. 126 (1), p. 012016. DOI: 10.1088/1757-899x/126/1/012016.
34. Efremenkov E.A., Martyushev N.V., Skeebe V.Yu., Grechneva M.V., Olisov A.V., Ens A.D. Research on the possibility of lowering the manufacturing accuracy of cycloid transmission wheels with intermediate rolling elements and a free cage. *Applied Sciences*, 2022, vol. 12 (1), p. 5. DOI: 10.3390/app12010005.
35. Martyushev N.V., Skeebe V.Yu. The method of quantitative automatic metallographic analysis. *Journal of Physics: Conference Series*, 2017, vol. 803 (1), p. 012094. DOI: 10.1088/1742-6596/803/1/012094.
36. Skeebe V.Yu., Ivancivsky V.V. Reliability of quality forecast for hybrid metal-working machinery. *IOP Conference Series: Earth and Environmental Science*, 2018, vol. 194 (2), p. 022037. DOI: 10.1088/1755-1315/194/2/022037.
37. Zverev E.A., Skeebe V.Yu., Skeebe P.Y., Khlebova I.V. Defining efficient modes range for plasma spraying coatings. *IOP Conference Series: Earth and Environmental Science*, 2017, vol. 87 (8), p. 082061. DOI: 10.1088/1755-1315/87/8/082061.
38. Mamadaliev R.A., Bakhmatov P.V., Martyushev N.V., Skeebe V.Yu., Karlina A.I. Influence of welding regimes on structure and properties of steel 12KH18N10T weld metal in different spatial positions. *Metallurgist*, 2022, vol. 65 (11–12), pp. 1255–1264. DOI: 10.1007/s11015-022-01271-9.
39. Balanovsky A.E., Shtayger M.G., Kondrat'ev V.V., Huy V. Van, Karlina A.I. Plasma-arc surface modification of metals in a liquid medium. *IOP Conference Series: Materials Science and Engineering*, 2018, vol. 411 (1), p. 012013. DOI: 10.1088/1757-899X/411/1/012013.
40. Karlina A.I., Karlina Y.I., Gladkikh V.A. Studying the microstructure, phase composition, and wear resistance of alloyed layers after laser surface melting of low-carbon steel 20. *Metallurgist*, 2024, vol. 68 (5), pp. 757–766. DOI: 10.1007/s11015-024-01782-7.
41. Karlina A.I., Karlina Y.I., Kondratiev V.V., Kononenko R.V., Breki A.D. Study of wear of an alloyed layer with chromium carbide particles after plasma melting. *Crystals*, 2023, vol. 13 (12), p. 1696. DOI: 10.3390/cryst13121696.
42. Balanovsky A.E., Shtayger M.G., Kondrat'ev V.V., Nebogin S.A., Karlina A.I. Complex metallographic researches of 110G13L steel after heat treatment. *IOP Conference Series: Materials Science and Engineering*, 2018, vol. 411 (1), p. 012014. DOI: 10.1088/1757-899X/411/1/012014.
43. Karlina A.I., Balanovskiy A.E., Kondratiev V.V., Romanova V.V., Batukhtin A.G., Karlina Y.I. An investigation into the behavior of cathode and anode spots in a welding discharge. *Applied Sciences Switzerland*, 2024, vol. 14 (21), p. 9774. DOI: 10.3390/app14219774.

Conflicts of Interest

The authors declare no conflict of interest.

© 2025 The Authors. Published by Novosibirsk State Technical University. This is an open access article under the CC BY license (<http://creativecommons.org/licenses/by/4.0>).